





Mapping of Ophiolitic Complex in Logar and Surrounding Areas (SE Afghanistan) With ASTER Data

Hemayatullah Ahmadi^{1,2}  · Kaan Kalkan³ 

Received: 14 February 2020 / Accepted: 1 February 2021 / Published online: 13 February 2021
© Indian Society of Remote Sensing 2021

Abstract

Ophiolites are the distinctive assemblage of mafic to ultramafic rocks and represent the abducted remnant of oceanic crust that was overthrust onto continental crust. Such types of rocks are rare around the world. One of the largest mafic–ultramafic complexes with an apparent area of about 2000 km² is in the southeast of Afghanistan between two active sinistral strike-slip faults within Logar and surrounding provinces. This study aims to discriminate, characterize, and separate the ophiolitic complex within Logar and adjacent regions in Afghanistan using Advanced Spaceborne Thermal Emission and Reflection Radiometer (ASTER) data. In this study, four different methods; Mineral Spectral Indices (SI), Band Ratios (BR), Relative Absorption Band Depth (RBD), and Spectral Angle Mapper (SAM), are applied to discriminate and separate the ophiolitic complex. SAM classifier is an efficient way to distinguish the selected surface mineral assemblage using USGS spectral library. The combination of SAM and refined MI yields efficient discrimination of mafic–ultramafic rocks with their alteration minerals around. Detailed mapping of the ophiolitic complex and associated rocks was achieved using refined MI, Band Ratio 4/8, and relative absorption band depth (RBD). The field works verified the results from ASTER data.

Keywords ASTER · Remote sensing · Mineral · Ophiolite · Mafic · Ultramafic

Introduction

Afghanistan has a complex geology and tectonic history due to its location in a region of the collision zone of Indian and Arabian plates with an almost stable Eurasian plate at the western end of the Himalayan mountain chain. This territory is composed of discrete tectonic crustal blocks and terranes bounded by active faults. These blocks are Gondwana, and Laurasia derived blocks, which have been accreted during the series of tectonic events related to the

Paleo-Tethys Ocean's closure in Jurassic to early Cretaceous times (Abdullah et al. 2008; Benham et al. 2009).

The concept of ophiolites was first developed in Europe in the early nineteenth century and went through several evolution phases (Dilek 2003). It is accompanied by mafic–ultramafic units in whose geological, mineralogical, and tectonic settings are not the same all over the crust.

According to Tapponnier et al. (1981), there are three extinct ophiolite complexes (Khost, Kabul, and Panjao) in Afghanistan related to post–Hercynian sutures. These complexes are located within the eastern and central regions of Afghanistan.

The Logar ophiolite complex is located about 30 km south of Kabul, Afghanistan, with an area of about 2000 km² between the Chaman and Gardiz (Altimur) left-lateral strike-slip faults. It is composed of lower Iherzolitic–dunitic–harzburgitic–gabbro ultramafic–mafic units that cross upward into a dolerite dyke complex, basaltic pillow lavas, and an uppermost sequence of volcanoclastic and terrigenous sedimentary units Fig. 1.

✉ Hemayatullah Ahmadi
h.ahmadi@kpu.edu.af; hahmadi@eskisehir.edu.tr

Kaan Kalkan
kaan.kalkan@tubitak.gov.tr

¹ Department of Geological Engineering and Exploration of Mines, Kabul Polytechnic University, Kabul, Afghanistan

² Department of Remote Sensing and GIS, Eskisehir Technical University, Eskisehir, Turkey

³ TÜBİTAK Space Technologies Research Institute, Ankara, Turkey

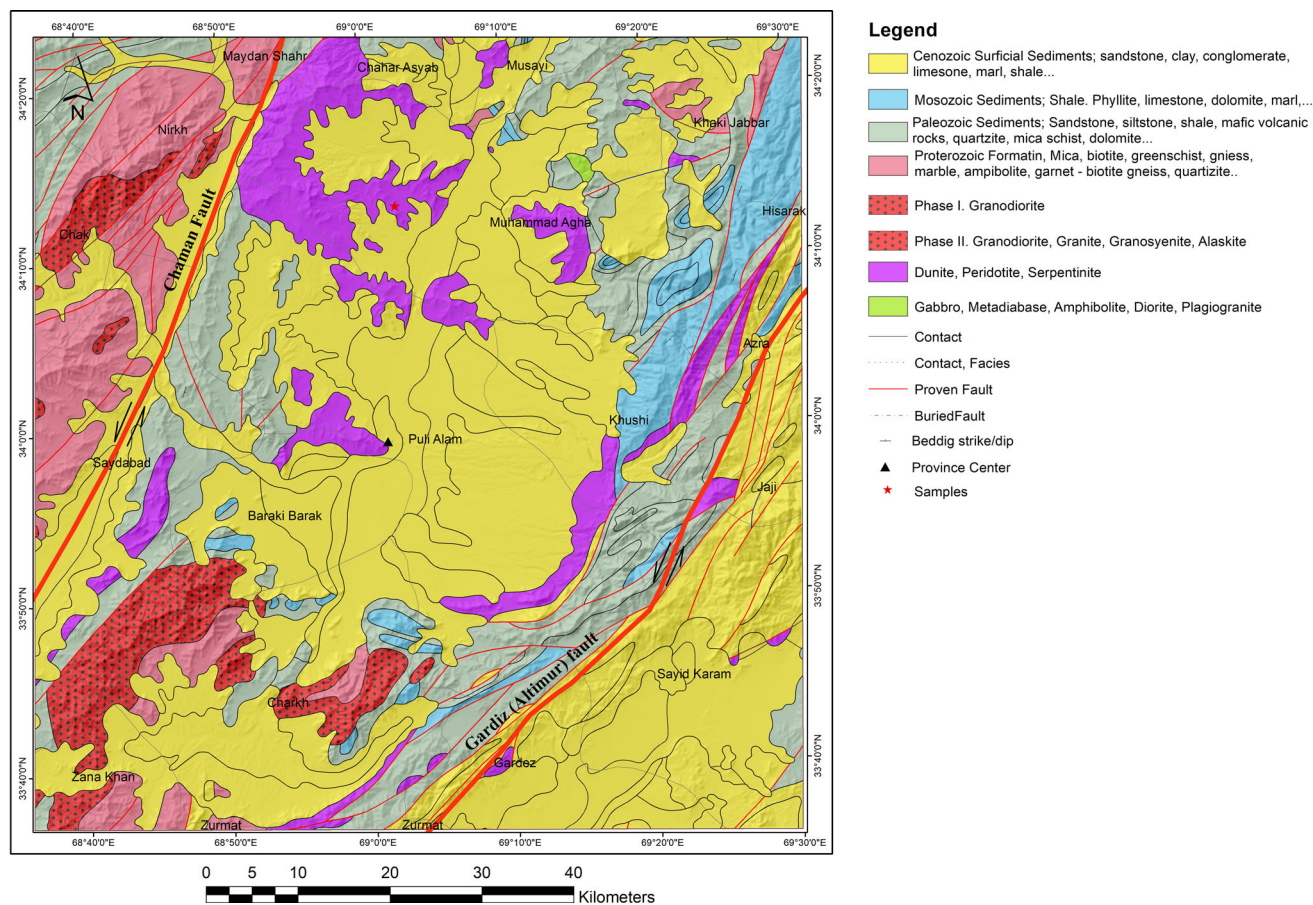


Fig. 1 The geological map of the study area (modified from Abdullah et al. 2008)

The rapid growth of remote sensing applications has affected research works in terms of high efficiency, low cost, and time-saving qualities. The improvements in remote sensing are achieved using various earth observation satellite data, digital image processing techniques, and the information extracted. This advancement provides the best opportunity for detailed mapping and understanding of the earth's surface in mineral exploration and tectonic structures. Several satellites are operating and being used for specific purposes such as; land observation, change detection, environmental geoscience, monitoring water quality, hydrology, mineral, and petroleum exploration, volcano science, earthquakes, floods, mass wasting hazards, and detailed mapping of high relief and remote areas (Pour et al. 2010).

ASTER, Landsat 8, Sentinel 2 are the optic remote sensing data that have widely been in geological studies, e.g., lithological mapping, stratigraphic sequences detection, hydrothermal alteration mapping, and structural analysis (Abdelmalik and Abd-Allah 2018; Abhary and Hassani 2016; Salem et al. 2018; Seleem et al. 2020; Shirazi et al. 2018). In this study, ASTER (Advanced Spaceborne Thermal Emission and Reflection Radiometer)

data were used for the digital image processing and information extraction.

Numerous studies have been conducted for the determination of ophiolitic zones and associated sequences using distinct remote sensing techniques, e.g., False Color Composite (FCC), Band Rationing (BR), Decorrelation stretch (DS), Spectral Angle Mapper (SAM), Spectral Indices, Minimum Noise Fraction (MNF) and Principle Component Analysis (PCA) (Abdelmalik and Abd-Allah 2018; Aboelkhair et al. 2020; Emam et al. 2016; Ge et al. 2018; Khaneghah and Arfania 2017; Seleem et al. 2020; R. Zhang and Zeng 2018).

Within the extend of the study area, a detailed study of ophiolitic complexes has not been researched. However, the Union of Soviet Socialist Republics (USSR), United States Geological Survey (USGS), and the colleagues from the geological engineering and exploration of mines department of Kabul Polytechnic University have carried out some limited studies. These studies are conventionally based and mainly focused on the ultramafic complexes of Afghanistan and PGE of Logar Ophiolite Complex (LOC) (Abdullah et al. 2008; Benham et al. 2009; Yousufi et al. 2019). A recent remotely sensed study by Abdelaziz et al.

(2018) used Landsat 8 OLI/TIRS for prospecting of Chromite in Logar massive. The authors in this study only applied FCC, BR, and PCA to discriminate the chromite masses.

Considering the applied methods in the literature, FCC and BR have widely been used to delineate ophiolitic complexes and associated lithologies. Using a single or two spatial method for demarcation of mafic–ultramafic layers may offer unreliable results due to the mineral's interference with similar absorption and reflection properties. Therefore, the integration of several approaches and selection of suitable imagery is considered the key factors to have reliable output results. This study examines the integration of several geospatial techniques, e.g., Spectral Indices (SI) for specific minerals, Band Ratio (BR), Relative Absorption Band Depth (RDB), and Spectral Angle Mapper (SAM) to ensure the validated mapping of ophiolitic masses in Logar and surrounding areas. This integration allows the complement/or validates the results of other methods.

Determination of ophiolite complexes is promising for understanding the petrology, mineralogy, and deep-seated oceanic lithosphere structure. Also, it leads to zones of mineralization that may have metallic and nonmetallic ore deposits (Zaigham and Mallick 2000). Conventional methods of ophiolite complexes within this area are time-consuming and expensive. Therefore, remote sensing techniques in such cases are considered a sufficient alternative. A comprehensive remote sensing study on the ophiolitic mapping of Logar province and surrounding area is lacking. Consequently, the objectives of this study are: (1) to discriminate ophiolitic complexes and associated altered surface minerals within the Logar and surrounding areas (SE of Afghanistan) using ASTER data, (2) to demonstrate the capability of ASTER imagery and applied remote sensing techniques in the demarcation of ophiolitic complexes, (3) to establish an integrated geospatial approach for targeting mafic–ultramafic minerals, and (4) to produce a final map showing the distribution of ophiolitic complexes and associated rock units.

Geologic Setting of Study Area

The study area (Logar and surrounding areas) is mainly located within the southern Kabul crustal block, the eastern part of the Helmand–Arghandab exotic terrane from the south and central Afghanistan. The study area's basement is composed of Central Afghanistan Terrane and platform-type cover sequence of Kabul block (Benham et al. 2009). The Kabul block is separated from Arghandab–Helmand block by the Chaman sinistral strike-slip fault and mostly accompanied by Neoproterozoic–Proterozoic basement and a

Phanerozoic platform-type carbonate sequence (Faryad et al. 2016).

According to Fig. 1, the most exposed rock formations are Cenozoic and Paleozoic sediments, mafic–ultramafic masses composed of dunite, peridotite, and serpentinite. The exact geologic age is not certainly identified; however, their ages are believed to be Cretaceous to Paleogene Period. The western part of the Chaman fault area is granite and granitoid complexes related to the Arghandab – Helmand terrane. The evidence of those granitic complexes also is exposed within the southwest of the study area near the Chaman fault.

The study concentrating on the exact emplacement mechanism of the Logar ophiolite complex has not been done yet. However, based on (Benham et al. 2009), the complex represents a fragment of the Mesozoic oceanic crust obducted onto the Kabul crustal block during the Himalayan orogeny is overlain by a volcanic–sedimentary sequence and accretionary prism sediments of Cretaceous age. To the north of the ophiolite complex, the Abparan thrust is reported by (Shareq et al. 1980) that separates the autochthonous Kabul block from the obducted Logar ophiolitic complex.

The main part of the Logar ophiolitic complex includes a large area of dunite and harzburgite with minor lherzolite, wehrlite, serpentinite, and serpentinite breccia. The upper part is accompanied by layered ultramafic to mafics, whereas the central region contains a dolerite dyke complex with steeply dipping or sub-vertical orientation (Benham et al. 2009).

The literature and past geological studies in this area showed the mafic–ultramafic complexes within the Logar region Fig. 1. In all the reviewed maps, these masses have been shown as a unit; however, their associated surface minerals have not been found in any geological maps. Detailed mapping concerning the ophiolitic rocks, their emplacement mechanism, tectonic structure, and associated mineral deposits are needed to study such complexes in detail concerning their associated minerals and the altered mafic and ultramafic minerals around them. In the current situation, compiling and providing such maps and materials in the region is problematic due to the uncertain insurgency situation. In this aspect, using remote sensing data is one of the most appropriate ways to get better and more reliable results.

Material and Methods

This study has been carried out by integrating ASTER data, and the previous field works data, and interpreting the whole country's geological map. ASTER data are characterized by spectral range, sufficient resolution, and high

spectral resolution in SWIR and TIR ranges. ASTER is multispectral imagery launched on the Terra platform of NASA Earth Observing System (EOS) in December 1999. Table 1 shows details (Emam et al. 2016; Fujisada 1995; Iwasaki et al. 2001; Yamaguchi et al. 1999).

Cloud free L1T ASTER tiles were downloaded, which were acquired in August 2007. Due to the broad coverage of the study area, seven different scenes are used in Table 2 downloaded for the study area.

We used ENVI 5.3 software for digital image analysis and ArcGIS 10.5 for vectorization and plotting purposes. This study's flow chart is given in Fig. 2, divided into three main steps: Preprocessing, processing, and post processing. Firstly, all the bands are radiometrically and atmospherically corrected. VNIR and SWIR bands were resampled to 30 m and stacked together to simplify the processing, and the TIR band was preprocessed as a separate dataset. All the analyses, information extraction steps, index calculations, and band ratios are included in the processing step, whereas the post processing step represents the validation and comparison of the extracted information with the field works and geological maps.

The following information extraction methods are tested in this study to provide a thematic map of ophiolitic rocks within the study area:

1. Spectral Indices for minerals
2. Band Rationing
3. Relative Absorption Band Depth
4. Spectral Angle Mapper

Moreover, the results are validated with the previous conventional data using a simple confusion matrix between the generated map and reference points.

Spectral Indices (BR)

The spectral indices are widely used in geological remote sensing to discriminate and delineate various minerals and rocks on the earth's surface. According to Jensen (2015); Sabins and Lulla (1987), this approach is likely to be similar to Principle Component Analysis (PCA). Both methods use the orthogonal transformation of multispectral data. Okyay (2012), in his M.Sc. thesis, stated that in PCA, the variance of multispectral data is maximized by the determination of axes mathematically, whereas in SI, the transformed axes are determined for a specific pattern.

Several SI is being used for ASTER (SWIR) and (TIR) bands for lithologic mapping. Based on the spectral characteristics of some minerals which having high reflectance within the SWIR portion of the electromagnetic spectrum., Ninomiya (2003) proposed (SWIR) spectral indices for determination of OH-bearing minerals (OHI), Kaolinite (KLI), Alunite (ALI), and Calcite (CLI). Since some minerals and rocks such as quartz and carbonate rocks cannot be sufficiently determined in VNIR—SWIR portions due to their high emission in thermal reflectance portion, Therefore, to overcome this problematic factor, Ninomiya et al. (2005) proposed specific SI; the Quartz Index (QI), the Carbonate Index (CI), and the Mafic Index (MI). Moreover, Ding et al. (2014) defined two indices for mafic-ultramafic rocks and two other indices for quartz-rich rocks according to TIR band ASTER using the Plank function.

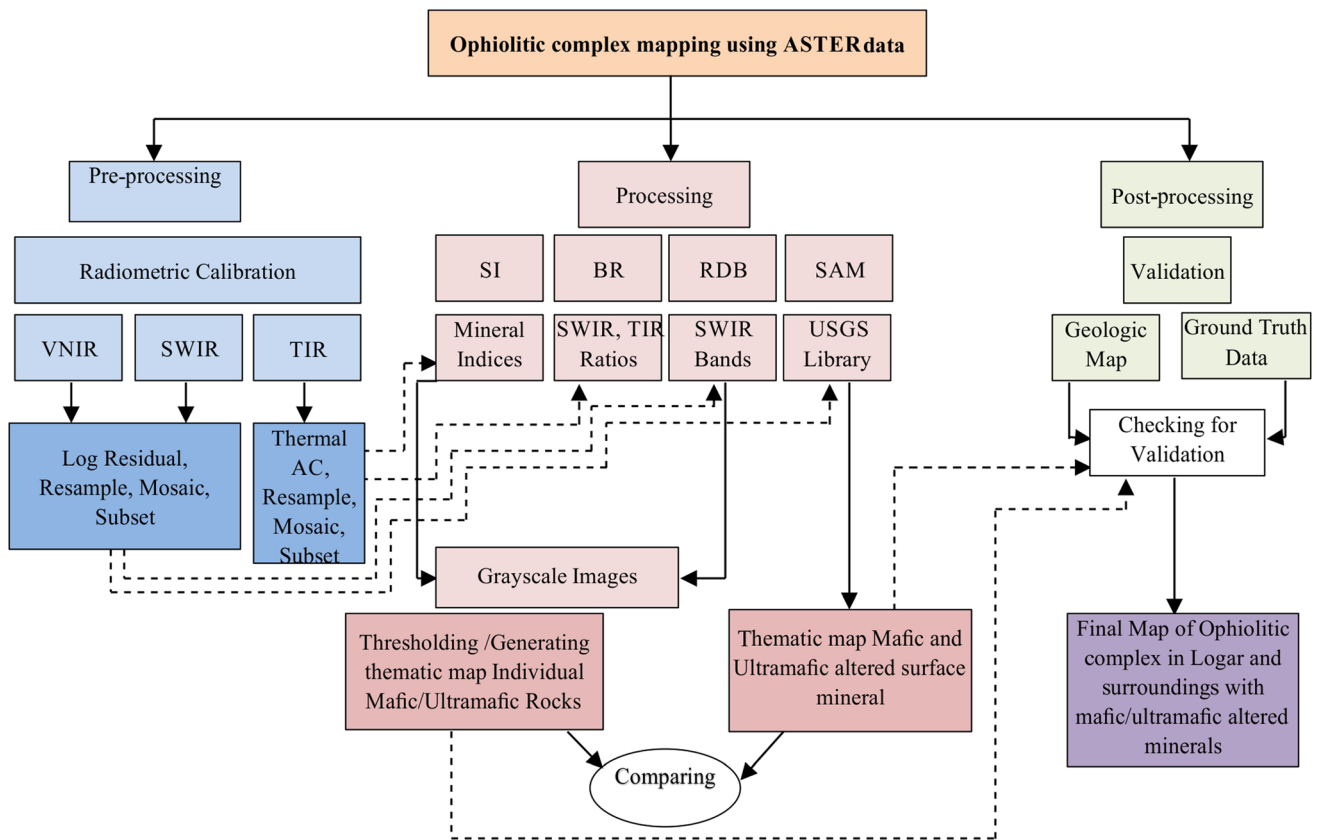
In this study, the mafic index (MI) of (Ninomiya et al. 2005) and two indices of Mafic – Ultramafic (M1, M2) from (Ding et al. 2014) have been calculated for mapping of the ophiolitic complex. The Mafic Index (MI) was calculated based on the following formula:

Table 1 Details of ASTER satellite imagery

Subsystems	Band No	Spectral range (μm)	Spatial resolution (m)	Radiometric resolution
VNIR	1	0.52–0.60	15	8 bits
	2	0.63–0.69		
	3 N	0.78–0.86		
	3B	0.78–0.86		
SWIR	4	1.60–1.70	30	8 bits
	5	2.145–2.185		
	6	2.185–2.225		
	7	2.235–2.285		
	8	2.295–2.365		
	9	2.360–2.430		
	TIR	10		
11		8.475–8.825		
12		8.925–9.275		
13		10.25–10.95		
14		10.95–11.65		

Table 2 The specifications of ASTER scenes downloaded for the study area

No	Tile ID	Latitude	Longitude	Acquisition date
1	AST_L1T_00307252007061829_20150520174617_112020	33.527	69.0712	2007/07/25
2	AST_L1T_00307252007061820_20150520174609_26699	34.0568	69.2228	2007/07/25
3	AST_L1T_00307252007061811_20150520174559_25240	34.5869	69.3773	2007/07/25
4	AST_L1T_00307182007061217_20150520154224_63135	33.6916	69.4976	2007/07/18
5	AST_L1T_00307022007061211_20150520031840_32098	33.7918	68.7725	2007/07/02
6	AST_L1T_00307022007061202_20150520031846_24528	34.3228	68.9119	2007/07/02
7	AST_L1T_00307182007061724_20150520152904_18864	34.0004	69.592	2007/07/18



Abbreviations

- SI – Spectral Mineral
- BR – Band Ratio
- RDB – Relative Absorption Band Depth
- SAM – Spectral Angle Mapper

Fig. 2 The flow chart of this study

$$MI = \frac{B12}{B13}$$

According to spectral properties of associated mafic–ultramafic rocks and sensitivity of carbonates, MI has been refined by Ninomiya et al. (2005) to reduce to effect of

carbonates Fig. 3a. The refined MI equation was calculated as follows:

$$MI = \frac{(B12 \times B14^3)}{B13^4}$$

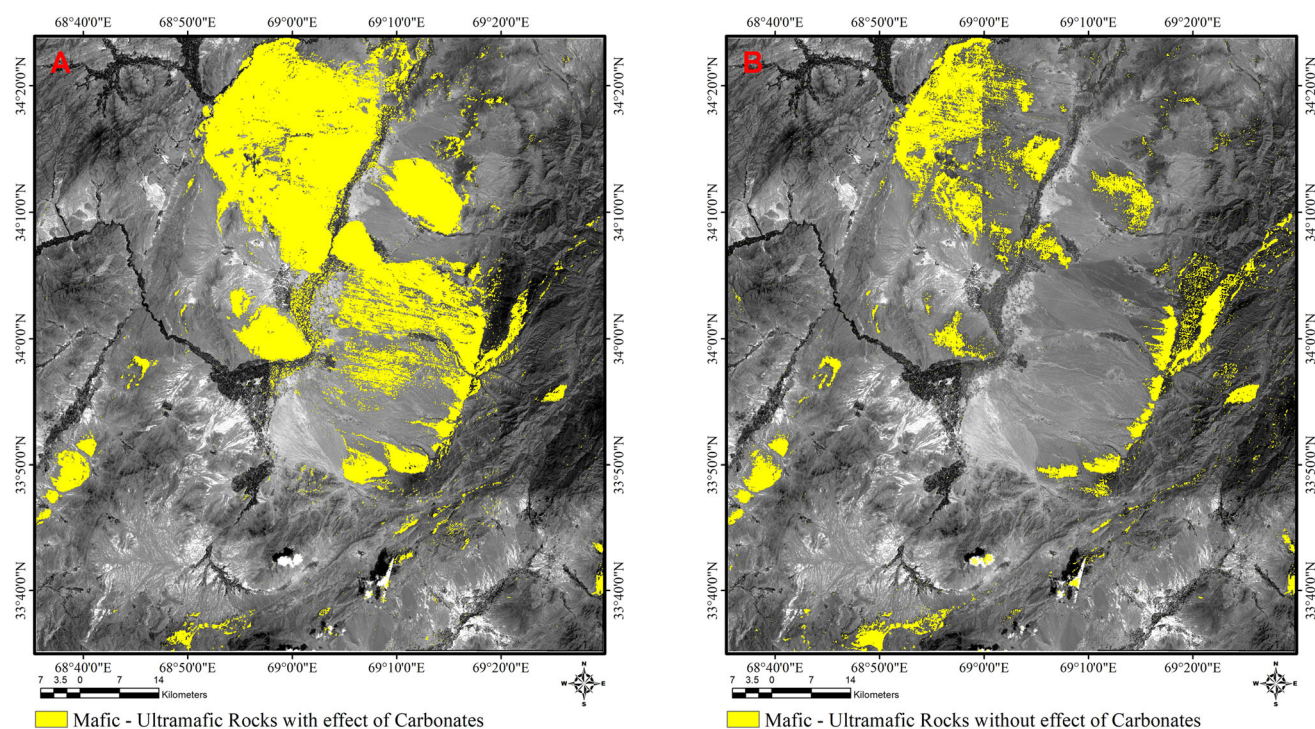


Fig. 3 The distribution of mafic–ultramafic rocks in the study area represented by yellow-colored pixels based on MI and refined version (Ninomiya et al. 2005); **a** The ophiolitic complex with the effect of carbonates, **b** The ophiolitic complex without the effect of carbonates

The generated image from the refined MI represents the mafic–ultramafic rocks by brighter pixels. The greyscale image was thresholded by a value of 0.89. Based on X. Zhang et al. (2003), the threshold value is assigned as $T = \mu + \sigma$ where μ is mean, and σ represents the standard deviation of digital numbers. Based on the formula, the value was calculated 0.88 accordingly, however using the trial and error method, it was found that 0.01 should be added to the calculated value because directly applying the calculated value mixed other pixels to pure pixels. In this study, we found that threshold values proposed by X. Zhang et al. (2003) methods cannot be applied directly to target the pure pixels; other minor values should be added or subtracted, respectively. The extracted informative pixels were saved and inserted on the ASTER – VNIR band 1 and plotted using ArcGIS 10.5 as depicted in Fig. 3.

For better effectiveness of ophiolitic rocks, the M1, M2 indices of Ding et al. (2014) were also calculated using the following equations:

$$M1 = (B13 - 0.9147) \times (B10 - 1.4366)$$

$$M2 = (B13 - 0.8945) \times (B11 - 1.2404)$$

The results from both mafic–ultramafic indices as brighter pixels on the greyscale image show the confusion of ophiolitic rocks with other rocks around. The mineralogical composition of ophiolitic rocks around the world is not fixed; therefore, these rocks' spectral characteristics

are also changing from region to region. Hence, the mafic–ultramafic rocks (ophiolitic complex) detected by the MI index were more reliable and accurate than the M1 and M2 index.

Band Ratios (BR)

Band ratio techniques effectively delineate and discriminate surface mineral types and vegetation density in remote sensing by dividing the greyscale image value in one band by the representing value in another band for each pixel in an image (Emam et al. 2016; Pour et al. 2010). It is widely used in geological studies to discriminate the rocks and minerals which cannot be seen in raw bands. This technique is utilized to enhance the spectral differences in bands and reduce the effects of topography (Inzana et al. 2003). The most widely used band ratios for ASTER VNIR—SWIR data are described by (Fu et al. 2007; Rowan et al. 2005); they are band ratio 2/1 for delineating iron oxide-rich minerals, band ratio 4/6 and 4/8 for highlighting the clay and carbonate minerals. According to mafic–ultramafic minerals' spectral properties, the TIR band ratio 12/14 is also calculated to discriminate mafic–ultramafic rocks (Yang et al. 2013).

In this study, two-band ratios (4/8 and 12/14) have been examined to discriminate the ophiolitic complex and associated rocks. The greyscale image generated by the

band ratio 4/8 was thresholded by the value 2 using the proposed method by X. Zhang et al. (2003) and trial and error approach, informative pixels were extracted from index image of band ratio 12/14 by threshold value greater than 1.062 which chosen by using error and trial methods and the proposed formula applied in the 4/8 band ratio. The carbonates extracted by 4/8 are mostly limestone, marl, dolomite, carbonated ultramafics, and some Quaternary surficial deposits mixed with carbonatic minerals. However, the mafic–ultramafic complex extracted by 12/14 seems to be not reliable as MI. for better clarification, extracted pixels of 4/8 ratio was overlaid with 12/14 ratio, and MI illustrated in Fig. 4a, b.

Relative Absorption Band Depth (RDB)

Relative band—depth (RDB) on images is calculated to detect the diagnostic mineral absorption features, while minimizing the reflectance variation related to topographic slope and albedo differences. It is widely used in geological remote sensing by the formulation of a three-point ratio for displaying AL—OL, Fe, Mg- OH, and CO₃ before conducting the detailed spectral analysis. RDB is the ratio of the numerator (S) that is the sum of the bands corresponding to the shoulders, and the denominator

representing the band located nearest the absorption feature minimum (M) (Emam et al. 2016; Yan et al. 2014).

$$RDB = \frac{(S_1 + S_2)}{M}$$

According to the above formula, RDB was calculated to discriminate the ophiolitic complex in detail for the study area. B6 and B9 have been selected as numerators, whereas B8 was select to represent the denominator in case of having the absorption peak for Fe, Mg–OH. The calculation was carried out as follows:

$$RDB = \frac{(B6 + B9)}{(B8^2)}$$

RDB's result as the grayscale image was thresholded by a value greater than 1.15 by calculating summation mean and standard deviation and examining the trial and error method to delineate mafic–ultramafic, superimposed on ASTER band 1 and shown in Fig. 5a.

Spectral Angle Mapper Algorithm (SAM)

The spectral angle mapper (SAM) algorithm is used based on the similarity of predefined classes' spectral properties and pixels on the image. It utilizes the spectral angle to determine the spectral similarity between an image pixel

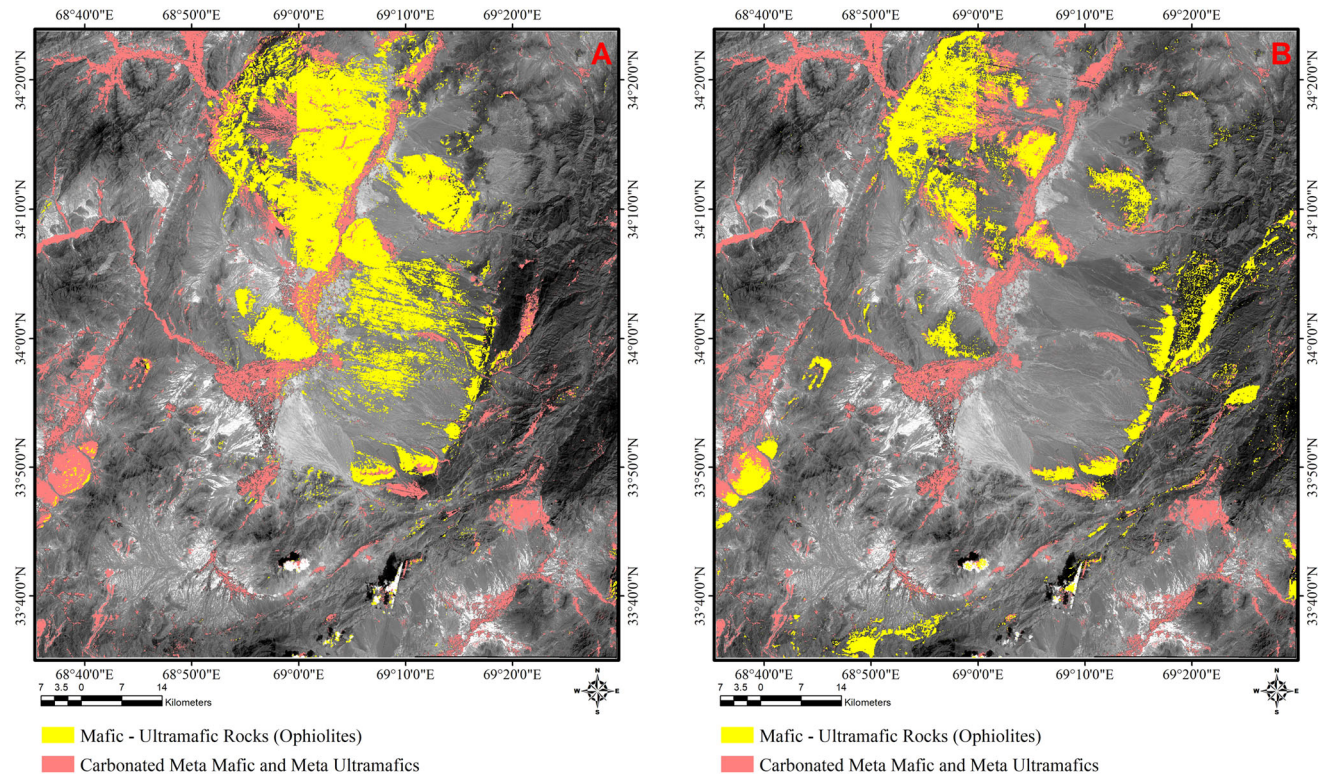


Fig. 4 The highlighted pixels representing ophiolitic complex and associated carbonates; **a** Ophiolitic complex extracted by 12/14 band ratio and carbonates by 4/8 band ratio; **b** Ophiolitic complex discriminated by MI and carbonates by 4/8 band ratio

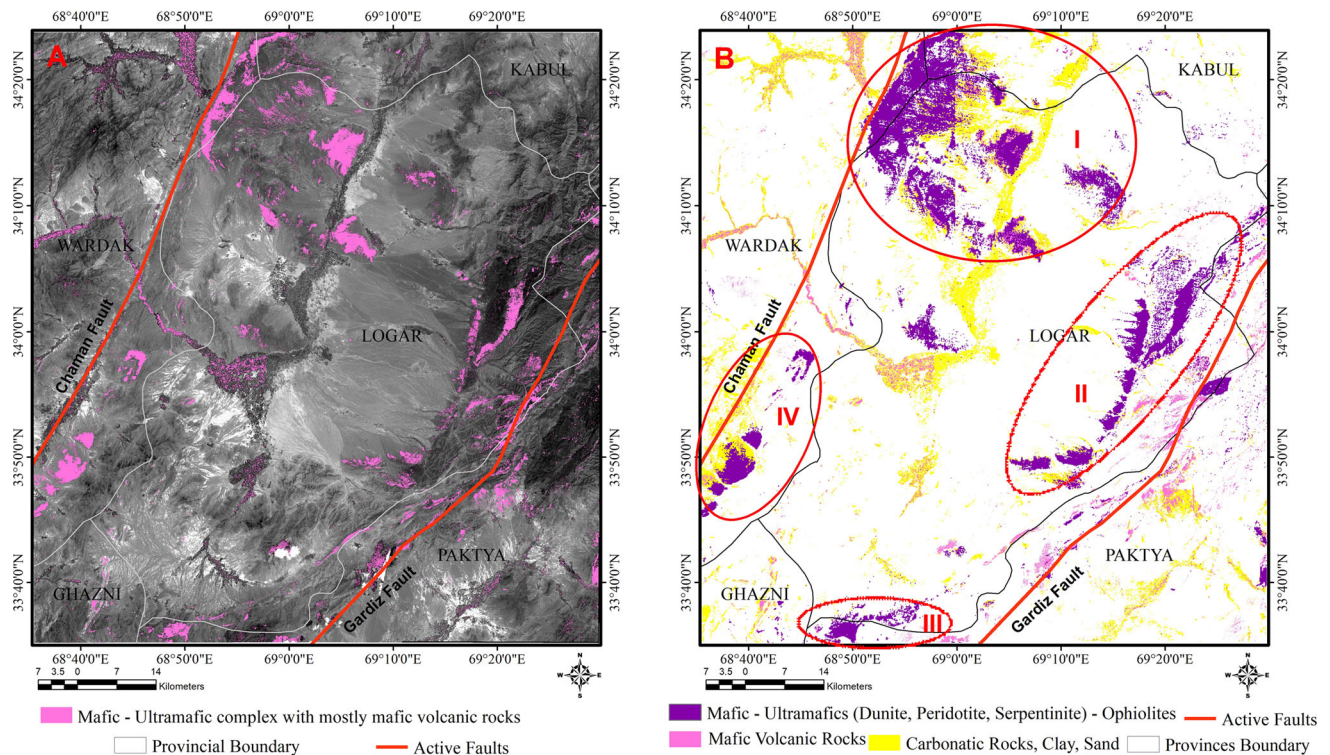


Fig. 5 The thematic map is showing the ophiolitic complex with associated active fault. **a** Mafic—Ultramafic (ophiolitic complex) with associated mafic volcanic fragments around generated by RDB.

spectrum and a reference spectrum in dimensional feature space with several available spectral bands (Weyermann et al. 2009; Yonezawa 2007). This algorithm was examined in the study area for the selected minerals using ENVI 5.3. The angle value was set as default by the software, which is (0.1 radians).

The algorithm was applied to determine the associated alteration minerals of mafic and ultramafic rocks, supporting ophiolitic rocks in the study area. The main minerals of ultramafic rocks are olivine and pyroxene. Due to hydrothermal alteration, these minerals are replaced by the serpentine group, mainly antigorite, chrysotile, and a lesser amount of brucite and talc (Emam et al. 2016; Hunt and Evarts 1981).

Mafic rocks are mainly composed of plagioclase, pyroxene, and olivine, which are altered to chlorite, epidote, calcite, iron oxides and hydroxides, and iron-rich minerals due to hydrothermal alteration (Emam et al. 2016).

Those mentioned above mafic-ultramafic alteration minerals have been selected as a reference using the USGS spectral library (Clark 1999) to be determined within the study area. The selected minerals were targeted to be determined between 0.556 and 2.4 μm since these minerals are distributed differently everywhere; therefore, USGS spectral library examined the different spectral types of the

b The combination of MI, 4/8 band ratio, and RDB highlighting the ophiolitic complex and carbonates

same minerals. The spectral signatures of selected Mafic and Ultramafic minerals are shown in Fig. 6.

Results and Discussion

In this study, four methods, including SI, BR, RBD, and SAM, were examined to discriminate the ophiolite complex within Logar and surrounding areas in great detail. Each method has its effectiveness; however, the refined MI proposed by Ninomiya et al. (2005) was found the most effective technique because it could separate the mafic-ultramafic rocks from other rock masses around. The carbonates, mostly dolomite, marl, limestone, have been reliably detected by the band ratio 4/8, which supports ophiolitic rocks' determination. RBD was found a more efficient method to highlight the ultramafic masses, and for accurate separation, it was combined with the results of refined MI and 4/8. The pure pixels of MI, band ratio 4/8, and RBD were combined in a single image to show the highly detailed ophiolitic complex and associated carbonates within Logar and surrounding regions. The result of the final combined map is depicted in Fig. 5b shows four large and small ophiolitic masses within Logar, Maidan Wardak, Paktya, and Kabul. The first large mass is shown in the Mohammad Agha district of Logar and partly within

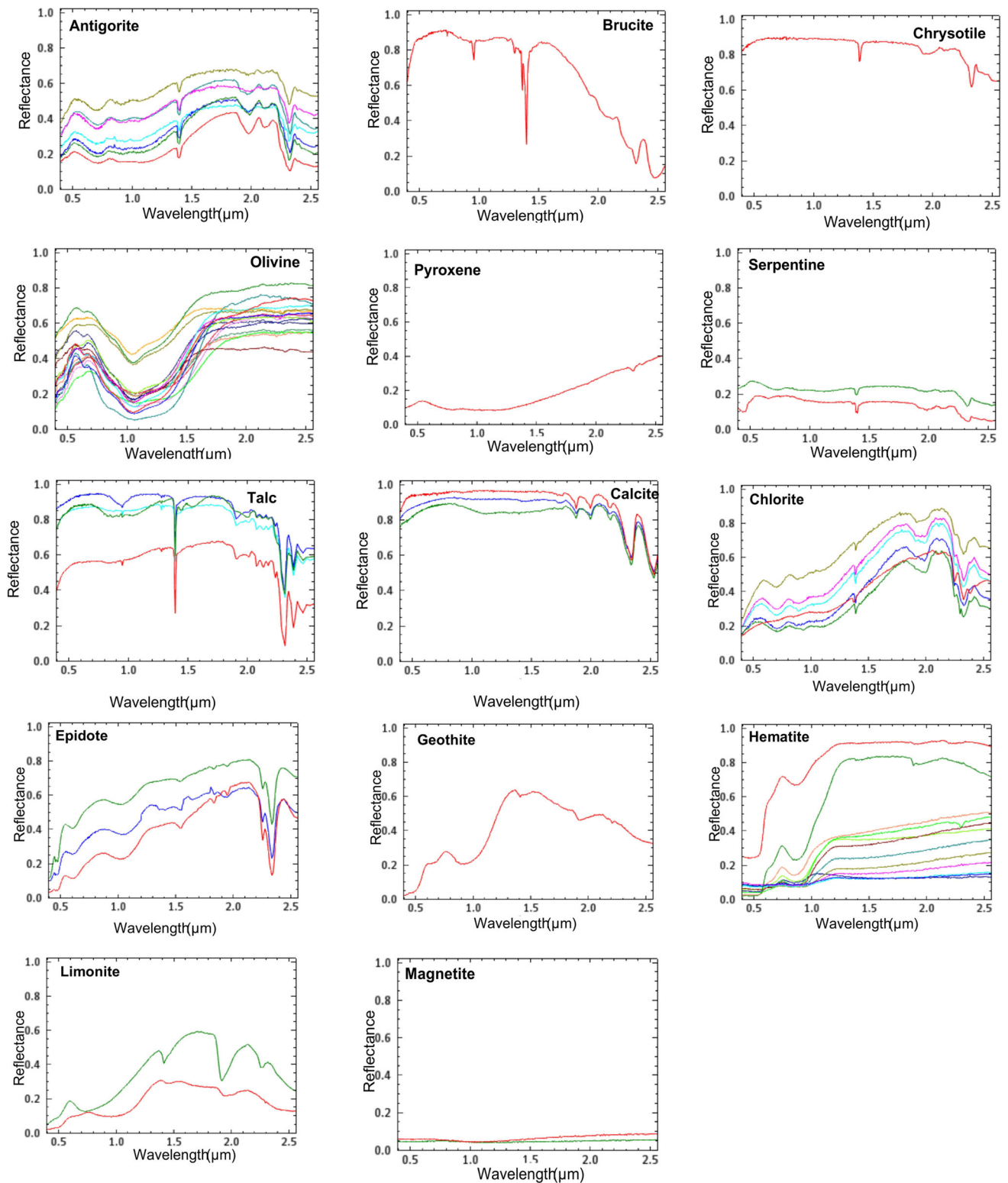


Fig. 6 The spectral signature of different mafic–ultramafic alteration minerals (extracted from USGS spectral library)a

Maidan Wardak province east of Chaman active fault Fig. 5I. The second large ophiolitic mass is lens-shaped, with a NE to SW trend discriminated in the east and center

of Logar province over the Khushi, and Poli Alam district, west of Altimur (Gardiz) sinistral strike-slip fault Fig. 5II. The third mass seems small that is located within Charkh of

Logar and the northern part of the Zurmat district of Pakya province. The mass is trending from east to west between Chaman and Altimur active strike-slip faults Fig. 5III. The fourth small ophiolitic mass has been determined along the east of Chaman fault within Sayed Abad district of Maidan Wardak province with NE to SW orientation. Figure 5IV Besides these complexes and masses, several other small patches occur in the Puli Alam of Logar and Sayed Karam, Gardiz, and Jaji districts of Paktya provinces accompanied by the indicators of active faults and mafic–ultramafic minerals.

The result of SAM algorithms is pure pixels showing the predefined classes. The generated thematic map of the SAM algorithm for the selected minerals over the study area shows that most of the regions are covered by sediments, rocks composed of carbonates such as calcite, dolomite. The distribution of antigorite is seen near the determined ophiolitic complexes. Also, these complexes have contact with talc occurrence over the Mohammad Agha and Khushi districts along the active faults Fig. 7.

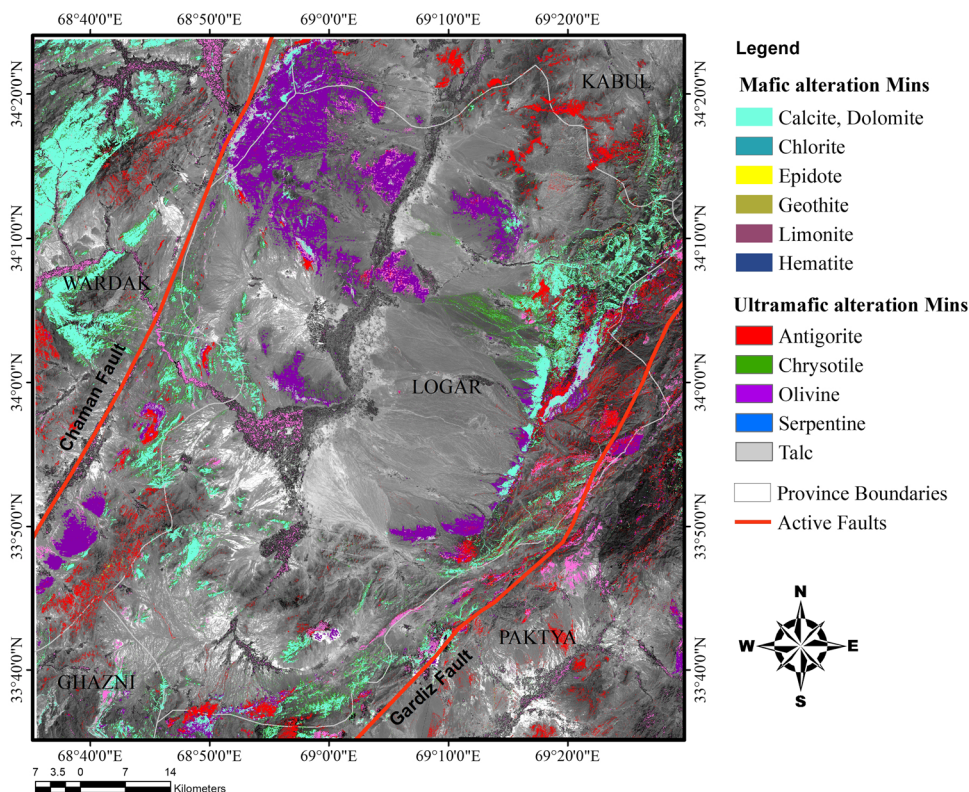
The determined ophiolitic rocks using ASTER data seem accurate and exact, which shows the capabilities of algorithms and approaches in this technology. This study is a comprehensive remotely sensed investigation over the ophiolitic rocks on Logar Ophiolite Complex. Previously, some limited research has been carried out on the specific mafic–ultramafic complex within the Mohammad Agha

district of Logar province. However, this study’s result reveals four large and small-large and small masses of ophiolitic rocks within Logar and surrounding areas of Maidan Wardak, Paktya, Kabul. These complexes may continue to other regions; however, they are out of this study’s scope.

Based on the comparison of the final thematic maps, Fig. 5. A and geological map Fig. 1 of the study area shown that ophiolitic masses detected by remote sensing-based mapping have more widespread distribution than the previously determined complex by traditional approaches. Photos of relevant regions support the result of mafic–ultramafic rocks obtained from remotely sensed data. Moreover, the ophiolitic rocks are the key indicators of chromite and other associated industrial minerals in a region. Therefore, to target and explore those industrial deposits and minerals, the ophiolitic complexes should be determined and characterized in detail with alteration minerals around. The previous studies showed up an only mafic–ultramafic complex of Logar with surficial deposits’ contact without describing the alteration minerals abundance. However, these alteration minerals in contact with mafic–ultramafic rocks were mapped, which most of them are distributed along with Chaman and Gardiz (Altimur) active left-lateral strike-slip faults.

Verification of the accuracy of a model applied by remote sensing-based studies depends on the results’

Fig. 7 The distribution of mafic–ultramafic alteration minerals detected by SAM



validation. The results obtained from these models demonstrate scientific significance when they are validated (Fabbri et al. 2003). Several methods are used for the validation of ophiolitic mapping via spectral and statistical approaches. In this study, two accuracy assessment approaches were applied: visual comparison with the geological map and creating a confusion matrix. The thematic information achieved from image processing was compared with the geological map of the study area compiled by Abdullah et al. (2008) Fig. 1 and field works sampled by Benham et al. (2009) Fig. 8. Total areas are compared between image processing algorithms and reference maps as an accuracy assessment. The compared parameters described in Table 3 shows better the capability of ophiolitic mapping using ASTER data. For accuracy assessment through the confusion matrix, about 120

reference points were collected for the previous conventional ophiolitic studies in Afghanistan (Abdullah et al. 2008; Benham et al. 2009; Siehl 2017; Tapponnier et al. 1981). The reference points were added to the validation map Fig. 8. The overlay layers showed that most of the reference points were overlapped with this study's results. The calculation confusion matrix of the reference and extracted data showed 78.33% of the overall accuracy with the 0.62 Kappa coefficient. The details of the user and producer accuracy are shown in Table 4. The overall accuracy and Kappa coefficient describe a substantial correlation between the extracted information from ASTER data and conventional data. Furthermore, the high producer and user accuracy for the ophiolite class, which is the main subject of this study, confirm extraction's correctness.

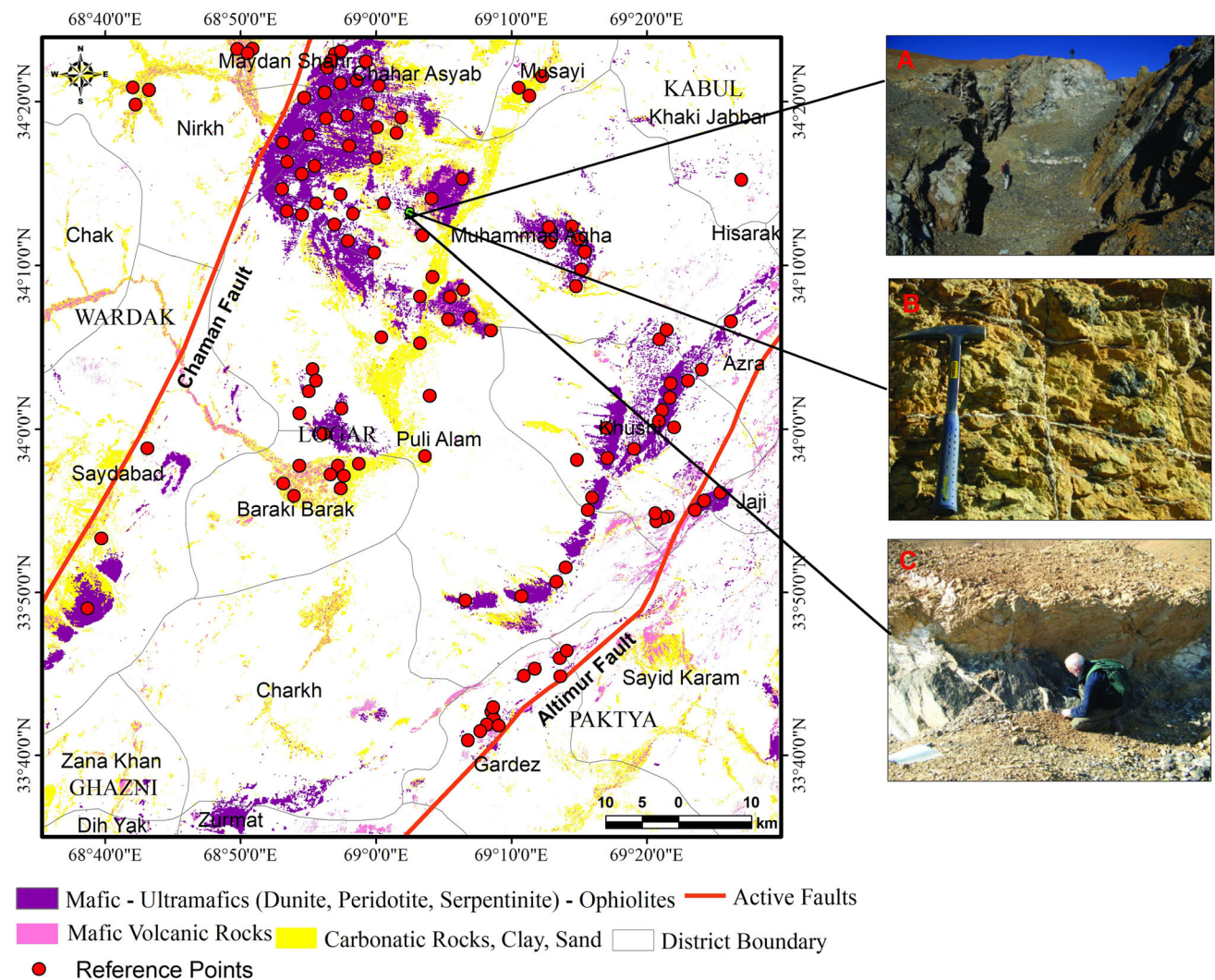


Fig. 8 The distribution of ophiolitic masses with associated rocks around; **a** the looking view of chromite mineralization with the layers of pyroxene (grey), dunite (brown), and carbonized ultramafic rocks

(white); **b** dunite mass with carbonatic veins and **c** The discordant location of pyroxene (grey) within dunite (brown) host rocks. Photo courtesy: (Benham et al. 2009)

Table 3 The comparative parameters for validation of the study

No	Parameters	Reference map	ASTER data	Remarks
1	Area (Km ²)	585.6	520.33	The area of ophiolitic rocks in ASTER data was calculated based on the pure pixels
2	Trending	Northeast	Northeast	The targeted ophiolitic masses are oriented parallel to Chaman and Gardiz active faults based on both data
3	Distribution	Mostly in Mohammad Agha district, Logar	Mostly in Mohammad Agha district, Logar	The main masses are situated in Logar; the rest is distributed in other surrounding areas. ASTER data shows the distribution of masses in some districts which are not seen in the reference map
4	Alteration Minerals	–	Mafic—Ultramafic	Besides the thematic map, a map of associated alteration surface minerals was provided, which can be a crucial indicator for further studies. However, these alteration minerals have not been depicted in the reference map

Table 4 Confusion matrix of the reference and extracted data

	Ophiolites	Carbonatic rocks, clay, sands	Mafic volcanic rocks	User accuracy
Ophiolites	57	7	5	82.61
Carbonatic rocks, clay, sands	12	22	0	64.71
Mafic volcanic rocks	0	2	15	88.24
Producer Accuracy	82.61	70.97	75.00	
Kappa Coefficient	0.62		Overall Accuracy 78.33	

Conclusion

Considering the main objective of this study, which was the mapping of ophiolitic rocks within the Logar and surrounding provinces in Afghanistan, four different remote sensing techniques, e.g., mineral spectral indices, band ratios, relative absorption band depth, and spectral angle mapper classification, were examined by using ASTER data.

The processing of ASTER imagery was a powerful tool for mapping the surficial lithology of arid and semi-arid regions, specifically in Afghanistan that mountainous areas and inappropriate situations make the fieldwork limited. Minerals have a different spectral signature; hence ASTER SWIR bands were found useful for delineating hydroxyl – bearing minerals such as clay, sulfate, and carbonate mineral groups, while TIR bands of ASTER was found sufficient to target quartz and discriminating rocks type specifically mafic–ultramafic rocks from others.

The mineral spectral indices have not resulted with the same result over all regions, hence in the Logar region, the refined (MI) developed by Ninomiya et al. (2005) was found the most efficient to target ophiolitic rocks. The identified ophiolitic masses are mostly in contact with carbonatic rocks and minerals, which show the abundance

of ultramafic carbonatization. The integration of several methods including SI, BR, RBD mapped four ophiolitic masses in the north, east, south, west of study area over the Chahar Asyab district of Kabul, Mohammad Agha, Khushi, Charkh and Puli Alam districts of Logar, Sayed Abad district of Maidan Wardak, and Sayed Karam, Jaji, and Zurmat districts of Paktya provinces, moreover, most of the determined ophiolitic complexes have NE—SW trending parallel to Chaman and Gardiz (Altimur) active sinistral strike-slip faults.

A detailed tectonic study in terms of these ophiolitic complexes' emplacement mechanism has not been done yet. Hence this work might help the further relevant studies; many metallic, nonmetallic mineral deposits are genetically associated with mafic–ultramafic complexes. Therefore, it is highly recommended to develop this study to explore more relevant deposits' perspectives, respectively.

Acknowledgments The authors thank Prof. Dr. John Shroder and anonymous reviewers for their constructive comments and suggestions that have developed the manuscript.

References

- Abdelaziz, R., Abd El-Rahman, Y., & Wilhelm, S. (2018). *Landsat-8 data for chromite prospecting in the Logar Massif, Afghanistan*: Heliyon. <https://doi.org/10.1016/j.heliyon.2018.e00542>.
- Abdelmalik, K. W., & Abd-Allah, A. M. A. (2018). Integration of remote sensing technique and field data in geologic mapping of an ophiolitic suture zone in western Arabian Shield. *Journal of African Earth Sciences*. <https://doi.org/10.1016/j.jafrearsci.2017.10.006>.
- Abdullah, S. H., Chmyriov, V. M., & Dronov, V. I. (2008). Geology and mineral resources of Afghanistan. *British Geological Survey- Occasional Publication No. 15. (Reprint of the 1980 English translation of the 1977 Russian publication)*.
- Abhary, A., & Hassani, H. (2016). Mapping hydrothermal mineral deposits using PCA and BR methods in Baft 1 100000 geological sheet Iran. *International Journal of Advanced Engineering Management and Science (IJAEMS)*, 2(9), 1433–1438.
- Abouelkhair, H., Abdelhalim, A., Hamimi, Z., & Al-Gabali, M. (2020). Reliability of using ASTER data in lithologic mapping and alteration mineral detection of the basement complex of West Berenice Southeastern Desert Egypt. *Arabian Journal of Geosciences*. <https://doi.org/10.1007/s12517-020-5227-x>.
- Benham, A. J., Kováč, P., Petterson, M. G., Rojkovic, I., Styles, M. T., Gunn, A. G., et al. (2009). Chromite and PGE in the logar ophiolite complex, Afghanistan. *Transactions of the Institutions of Mining and Metallurgy, Section B: Applied Earth Science*, 118(2), 45–58. <https://doi.org/10.1179/174327509X434957>.
- Clark, R. N. (1999). *Spectroscopy of rocks and minerals, and principles of spectroscopy*. Remote sensing for the earth sciences: Manual of remote sensing.
- Dilek, Y. (2003). Ophiolite concept and its evolution. *Special Paper of the Geological Society of America*, 373, 1–16. <https://doi.org/10.1130/0-8137-2373-6.1>.
- Ding, C., Liu, X., Liu, W., Liu, M., & Li, Y. (2014). Mafic-ultramafic and quartz-rich rock indices deduced from ASTER thermal infrared data using a linear approximation to the planck function. *Ore Geology Reviews*. <https://doi.org/10.1016/j.oregeorev.2014.01.005>.
- Emam, A., Zoheir, B., & Johnson, P. (2016). ASTER-based mapping of ophiolitic rocks: Examples from the Allaqi-Heiani suture. *SE Egypt International Geology Review*, 58(5), 525–539. <https://doi.org/10.1080/00206814.2015.1094382>.
- Fabbri, A., Chung, C.-J.F., & Fabbri, A. G. (2003). Validation of spatial prediction models for landslide hazard mapping. *Natural Hazards*, 30(3), 451–472. <https://doi.org/10.1023/B:NHAZ.0000007172.62651.2b>.
- Faryad, S. W., Collett, S., Finger, F., Sergeev, S. A., Čopjaková, R., & Siman, P. (2016). The Kabul Block (Afghanistan), a segment of the Columbia Supercontinent, with a Neoproterozoic metamorphic overprint. *Gondwana Research*, 34, 221–240. <https://doi.org/10.1016/j.gr.2015.02.019>.
- Fu, B., Zheng, G., Ninomiya, Y., Wang, C., & Sun, G. (2007). Mapping hydrocarbon-induced mineralogical alteration in the northern Tian Shan using ASTER multispectral data. *Terra Nova*, 19(4), 225–231. <https://doi.org/10.1111/j.1365-3121.2007.00739.x>.
- Fujisada, H. (1995). Design and performance of ASTER instrument. Proceedings of SPIE. *The International Society for Optical Engineering*, (2583), Int. Soc. Opt. Eng. <https://www.spiedigitallibrary.org/conference-proceedings-of-spie/2583/0000/Design-and-performance-of-ASTER-instrument/> Retrieved Nov 29 2020 from <https://doi.org/10.1117/12.228565.short>.
- Ge, W., Cheng, Q., Jing, L., Armenakis, C., & Ding, H. (2018). Lithological discrimination using ASTER and Sentinel-2A in the Shibanjing ophiolite complex of Beishan orogenic in Inner Mongolia. *China. Advances in Space Research*, 62(7), 1702–1716. <https://doi.org/10.1016/j.asr.2018.06.036>.
- Hunt, G. R., & Evarts, R. C. (1981). Use of near-infrared spectroscopy to determine the degree of serpentinization of ultramafic rocks. *Geophysics*, 46(3), 316–321. <https://doi.org/10.1190/1.1441202>.
- Inzana, J., Kusky, T., Higgs, G., & Tucker, R. (2003). Supervised classifications of Landsat TM band ratio images and Landsat TM band ratio image with radar for geological interpretations of central Madagascar. *Journal of African Earth Sciences*, 37(1–2), 59–72. [https://doi.org/10.1016/S0899-5362\(03\)00071-X](https://doi.org/10.1016/S0899-5362(03)00071-X).
- Iwasaki, A., Fujisada, H., Akao, H., Shindou, O., & Akagi, S. (2001). Enhancement of spectral separation performance for ASTER/SWIR. Proceedings of SPIE. In *International Society for Optical Engineering*. <https://www.spiedigitallibrary.org/conference-proceedings-of-spie/4486/0000/Enhancement-of-spectral-separation-performance-for-ASTER-SWIR/> Retrieved Nov 29 2020 from <https://doi.org/10.1117/12.455140.short>.
- Jensen, J. R. (2015). Introductory digital image processing: a remote sensing perspective. Second edition. Introductory digital image processing: a remote sensing perspective. Second edition (4th Edition).
- Khaneghah, A. R. N., & Arfania, R. (2017). Lithological analysis of nain ophiolitic zone using ASTER data. *Open Journal of Geology*, 07(08), 1200–1214. <https://doi.org/10.4236/ojg.2017.78080>.
- Ninomiya, Y. (2003). Rock type mapping with indices defined for multispectral thermal infrared ASTER data: Case studies. *Remote Sensing for Environmental Monitoring, GIS Applications, and Geology*. <https://doi.org/10.1117/12.462358>.
- Ninomiya, Y., Fu, B., & Cudahy, T. J. (2005). Detecting lithology with advanced spaceborne thermal emission and reflection radiometer (ASTER) multispectral thermal infrared “radiance-at-sensor” data. *Remote Sensing of Environment*. <https://doi.org/10.1016/j.rse.2005.06.009>.
- Okyay, Ü. (2012). *Lithologic discrimination and mapping by aster thermal infrared imagery*. Turkey: Middle East Technical University.
- Pour, A. B., Hashim, M., & Marghany, M. (2010). Characterization of ASTER Data for Mineral Exploration. In MRSS 6th international remote sensing & gis conference and exhibition (p. 6). Retrieved Nov 29 2020 from <https://www.academia.edu/download/30703706/130-MRSS-Amin-Beiranvand-Pour.pdf>.
- Rowan, L. C., Mars, J. C., & Simpson, C. J. (2005). Lithologic mapping of the Mordor, NT, Australia ultramafic complex by using the advanced spaceborne thermal emission and reflection radiometer (ASTER). *Remote Sensing of Environment*, 99(1–2), 105–126. <https://doi.org/10.1016/j.rse.2004.11.021>.
- Sabins, S., & Lulla, K. (1987). Remote sensing: Principles and interpretation. *Geocarto International*. <https://doi.org/10.1080/10106048709354087>.
- Salem, S. M., ElSharkawi, M. A., ElAlfy, Z., & Ahmed, S. E. (2018). The use of ASTER data and geochemical analyses for the exploration of gold at Samut area South Eastern Desert of Egypt. *Arabian Journal of Geosciences*. <https://doi.org/10.1007/s12517-018-3793-y>.
- Seleem, T., Hamimi, Z., Zaky, K., & Zoheir, B. (2020). ASTER mapping and geochemical analysis of chromitite bodies in the Abu Dahr ophiolites, South Eastern Desert. *Egypt Arabian Journal of Geosciences*, 13(15), 1–21. <https://doi.org/10.1007/s12517-020-05624-z>.
- Shareq, A., Voinov, V. N., Nevretdinov, E. B., Kubatkin, L. V., & Gusav, I. A. (1980). The Logar ultrabasite massif and its reflection in the magnetic field (East Afghanistan). *Tectonophysics*. [https://doi.org/10.1016/0040-1951\(80\)90070-0](https://doi.org/10.1016/0040-1951(80)90070-0).

- Shirazi, A., Hezarkhani, A., & Shirazy, A. (2018). Remote sensing studies for mapping of iron oxide regions, South of Kerman, IRAN. *International Journal of Science and Engineering Applications*, 7(4), 045–051. <https://doi.org/10.7753/ijsea0704.1002>.
- Siehl, A. (2017). Structural setting and evolution of the Afghan orogenic segment—A review. *Geological Society Special Publication*, 427, 57–88. <https://doi.org/10.1144/SP427.8>.
- Tapponnier, P., Mattauer, M., Proust, F., & Cassaigneau, C. (1981). Mesozoic ophiolites, sutures, and large-scale tectonic movements in Afghanistan. *Earth and Planetary Science Letters*. [https://doi.org/10.1016/0012-821X\(81\)90189-8](https://doi.org/10.1016/0012-821X(81)90189-8).
- Weyermann, J., Schläpfer, D., Hueni, A., Kneubühler, M., & Schaepman, M. (2009). Spectral angle mapper (SAM) for anisotropy class indexing in imaging spectrometry data. *Imaging Spectrometry XIV*. doi, 10(1117/12), 825991.
- Yamaguchi, Y., Fujisada, H., Kudoh, M., Kawakami, T., Tsu, H., Kahle, A. B., & Pniel, M. (1999). ASTER instrument characterization and operation scenario. *Advances in Space Research*. [https://doi.org/10.1016/S0273-1177\(99\)00293-8](https://doi.org/10.1016/S0273-1177(99)00293-8).
- Yan, J., Zhou, K., Liu, D., Wang, J., Wang, L., & Liu, H. (2014). Alteration information extraction using improved relative absorption band-depth images, from HJ-1A HSI data: A case study in Xinjiang Hatu gold ore district. *International Journal of Remote Sensing*. <https://doi.org/10.1080/01431161.2014.963896>.
- Yang, Q., Liu, X., Li, X., Ding, C., & Yang, F. (2013). Lithology identification of the North Qilian belt by surface temperature and spectral emissivity information derived from ASTER TIR Data. *International Journal of Remote Sensing Applications*, 3(4), 235. <https://doi.org/10.14355/ijrsa.2013.0304.09>.
- Yonezawa, C. (2007). Maximum likelihood classification combined with spectral angle mapper algorithm for high resolution satellite imagery. *International Journal of Remote Sensing*. <https://doi.org/10.1080/01431160701373713>.
- Yousufi, A., Bekbotayeva, A., Muszynski, A., Ahmadi, H., & Baibatscha, A. (2019). Distribution of ultramafic complexes in Afghanistan. *International Multidisciplinary Scientific GeoConference Surveying Geology and Mining Ecology Management, SGEM*, 19, 163–170. <https://doi.org/10.5593/sgem2019/1.1/S01.020>.
- Zaigham, N. A., & Mallick, K. A. (2000). Bela ophiolite zone of southern Pakistan: Tectonic setting and associated mineral deposits. *Bulletin of the Geological Society of America*. <https://doi.org/10.1130/0016-7606>.
- Zhang, X., Friedl, M. A., Schaaf, C. B., Strahler, A. H., Hodges, J. C. F., Gao, F., et al. (2003). Monitoring vegetation phenology using MODIS. *Remote Sensing of Environment*. [https://doi.org/10.1016/S0034-4257\(02\)00135-9](https://doi.org/10.1016/S0034-4257(02)00135-9).
- Zhang, R., & Zeng, M. (2018). Mapping lithologic components of ophiolitic mélanges based on ASTER spectral analysis A case study from the Bangong-Nujiang Suture Zone (Tibet, China). *ISPRS International Journal of Geo-Information*. <https://doi.org/10.3390/ijgi7010034>.

Publisher's Note Springer Nature remains neutral with regard to jurisdictional claims in published maps and institutional affiliations.